Constant contour integration in peripheral vision for stimuli with good Gestalt properties

Shu-Guang Kuai

State Key Laboratory of Cognitive Neuroscience and Learning, Beijing Normal University, Beijing, China, & Institute of Neuroscience, Chinese Academy of Sciences, Shanghai, China

Cong Yu

State Key Laboratory of Cognitive Neuroscience and Learning, Beijing Normal University, Beijing, China, & Institute of Neuroscience, Chinese Academy of Sciences, Shanghai, China

The visual system integrates discrete but aligned local stimuli to form percept of global contours. Previous experiments using "snake" contours showed that contour integration was mainly present in foveal vision but absent or greatly weakened in peripheral vision. In this study, we demonstrated that, for contour stimuli such as circles and ellipses, which bore good Gestalt properties, contour integration for shape detection and discrimination was nearly constant from the fovea to up to 35° visual periphery! Contour integration was impaired by local orientation and position jitters of contour elements, indicating that the same local contour linking mechanisms revealed with snake contour stimuli also played critical roles in integration of our good Gestalt stimuli. Contour integration was also unaffected by global position jittering up to 20% of the contour size and by dramatic shape jittering, which excluded non-contour integration processes such as detection of various local cues and template matching as alternative mechanisms for uncompromised peripheral perception of good Gestalt stimuli. Peripheral contour integration also presented an interesting upper–lower visual field symmetry after asymmetries of contrast sensitivity and shape discrimination were discounted. The constant peripheral performance might benefit from easy detection of good Gestalt stimuli, which popped out from background noise, from a boost of local contour linking by top–down influences and/or from multielement contour linking by long-range interactions.

Keywords: contour integration, peripheral vision, good Gestalt

Introduction

Humans can perceive global contours from properly aligned local stimulus elements imbedded in a random stimulus field (Field, Hayes, & Hess, 1993; Geisler, Perry, Super, & Gallogly, 2001; Kapadia, Westheimer, & Gilbert, 2000; Kovacs & Julesz, 1993; Li, 1998; Sigman, Cecchi, Gilbert, & Magnasco, 2001; see Hess & Field, 1999; Hess, Hayes, & Field, 2003 for recent reviews). This contour integration process represents important sensation to perception transition and is a fundamental component of object processing. It also plays a critical role in perception of natural images because of the edge co-occurrence statistical properties of contours in nature images (Geisler et al., 2001; Sigman et al., 2001) and, thus, serves an important function for everyday vision.

Existing experimental evidence suggests that contour integration is mainly present in foveal vision and is absent (Hess & Dakin, 1997) or greatly weakened (Nugent, Keswani, Woods, & Peli, 2003) in peripheral vision. Hess and Dakin (1997) first reported that peripheral contour integration for "snake" contours (Figure 1a) was entirely missing beyond 10° retinal eccentricity. They found that peripheral contours consisting of same-phase elements could be detected effortlessly by their observers, but those consisting of alternating-phase elements were undetectable. A single-filter model, which implied no integration of multiple filter responses, was thus proposed to explain peripheral contour detection (Hess & Dakin, 1997). This model would not respond to contours formed by alternating-phase elements, which would have been averaged out. More recently, Nugent et al. (2003) used identical stimuli to study peripheral contour integration, but they reported that contour integration declined gradually and diminished near 30° retinal eccentricity. Moreover, the performance differences for same-phase and alternating-phase stimuli were very small, which argued against Hess and Dakin's single-filter model. However, regardless of the discrepancies of experimental results in many ways, both studies reached a consensus for poor peripheral contour integration, which became absent beyond a certain retinal eccentricity. On the other hand, Hess and Dakin (1999) discounted local position uncertainty of contour elements as an alternative account to their single-filter model. They measured equivalent positional noise for contour elements across the visual field and found that equating position uncertainty, while reducing foveal contour integration performance, was

doi: 10.1167/6.12.7 Received March 12, 2006; published December 15, 2006 ISSN 1534-7362

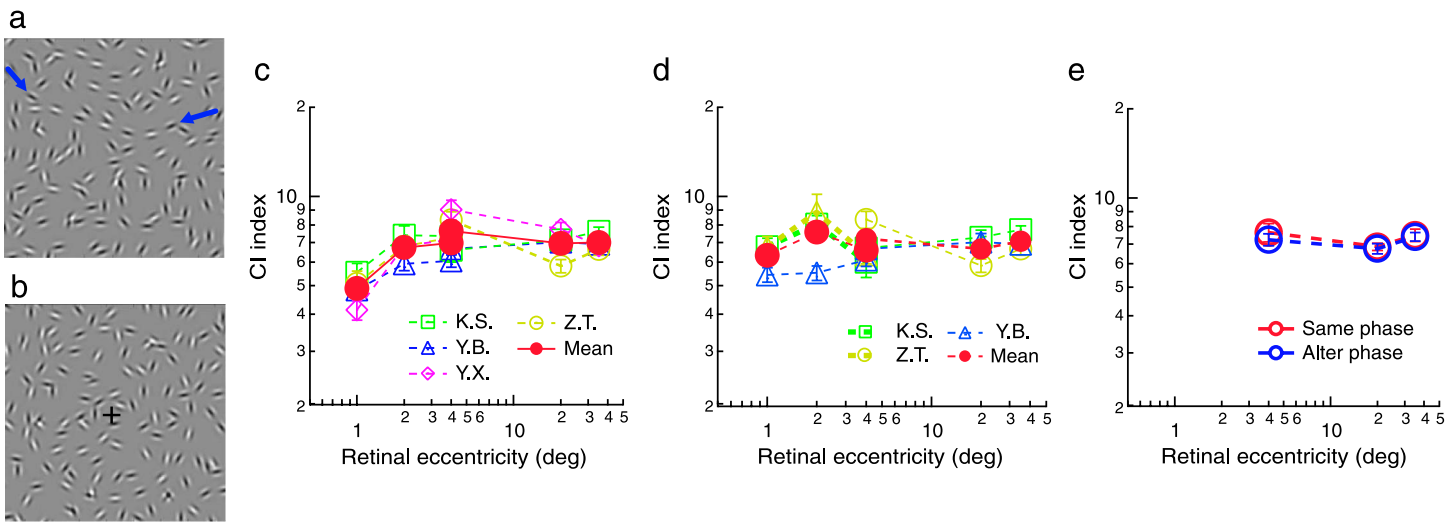

Figure 1. Contour integration for detection in peripheral vision. (a) An example of snake contour stimuli used in earlier studies (Hess & Dakin, 1997; Nugent et al., 2003), with the contour path indicated by arrows. (b) Stimuli used in contour detection experiments: a circular contour imbedded in a random Gabor noise field. (c) Individual and mean contour integration indices for contour detection at various retinal eccentricities. Error bars in this figure as well as in subsequent ones indicate standard error of the mean. (d) Same as Panel c except that lower spatial frequencies were used for stimuli presented at 1–4° retinal eccentricities. The 4–35° individual data are the same as in Panel c for three participating observers. (e) The effect of relative phase between neighboring contour elements on contour integration averaged from three additional observers.

insufficient to explain poor contour integration in the visual periphery.

We suspected that poor contour performance might be specific to the stimuli used in these studies. Both Hess and Dakin (1997) and Nugent et al. (2003) used snake contours (Figure 1a) that changed their directions from element to element randomly. Their global directions were also uncertain from trial to trial. These snake contours tended to have weaker integration than did contours that curved in one direction (Pettet, 1999; Pettet, McKee, & Grzywacz, 1998; Tversky, Geisler, & Perry, 2004) or were closed in ends like circles (Braun, 1999; Kovacs & Julesz, 1993; Pettet, 1999). Top–down influences from higher levels and other factors might facilitate contour integration of these "good Gestalt" stimuli (see the Discussion section). In the visual periphery, weaker contour integration for snake stimuli might have been masked by peripheral position uncertainty of the contour stimuli and by other factors (Orbach & Wilson, 1999), but good Gestalt contour stimuli could override these masking effects.

We set to investigate whether and how circular and elliptical contours that had good Gestalt properties could be integrated in the visual periphery. Circular contours also had an additional advantage for its unambiguous retinal position because all contour elements were placed in the same retinal eccentricity when the observers fixated on the center of the circle. In contrast, the retinal position of a snake contour only made sense as the eccentricity value of the center contour element while other elements spread out in the visual field (Hess & Dakin, 1997; Nugent et al., 2003).

Methods

Observers and apparatus

Twelve observers with normal or corrected-to-normal vision participated in this study. Most observers performed some of the experiments. All observers except K.S. were new to psychophysical experiments and unaware of the purposes of the experiments. All observers received training before data collection.

The stimuli were generated in real time by a Matlab-based WinVis program (Neurometrics Institute, Oakland, CA, USA) and presented on a 21-in. Dell P1130 color monitor (1,024 × 768 pixel, 0.37 × 0.37 mm per pixel, 120 Hz frame rate, 40 cd/m^2 mean luminance). Luminance of the monitor was linearized by an 8-bit lookup table. Experiments were run in a dimly lit room.

Stimuli and procedure

The stimuli were a full-screen field of randomly distributed and randomly oriented Gabors (Gaussian windowed sinusoidal gratings), within which a circular or elliptical contour formed by additional equal-spacing Gabor elements might imbed (Figures 1b and 2a). The screen was divided into 17 × 12 invisible square grids (204 in total) for stimuli presented in 1°, 2°, and 4° retinal eccentricities and into 28 × 21 grids (588 in total) for stimuli in 4°, 20°, and 35° retinal eccentricities. The

center of each random Gabor was randomly positioned within ±0.5 grid size in both horizontal and vertical directions from the grid center; hence, in the extreme cases, half of the Gabor would overlap with the neighboring grid. A contour element would replace a random Gabor element in the same grid to get rid of density cues. In contour detection tasks (see below), the same contour stimuli were also shown in the nontarget image, but the equal-spacing contour elements were randomly repositioned along the contour path and were randomly oriented. This manipulation would further avoid local density cues around the contour stimuli. The stimulus images were regenerated for each interval within a 2AFC trial (see below) and across each trial. The locations of the equal-spacing contour elements varied along the contour path from image to image. The randomly oriented and randomly placed background Gabors were rerandomized in each new image. All Gabors, whether random or contour elements, were physically identical except for their locations, orientations, and phases. The phases of neighboring contour elements typically alternated at 0° and 180°, whereas the phases of random Gabors randomized at 0° or 180°. The contour was typically centered on the full-screen Gabor field (except in global position jitter conditions, Figure 4a); thus, for circular contours, the elements were located at the same retinal eccentricity. The standard deviation of the Gabor Gaussian envelope (σ) was always equal to 0.425 times the Gabor wavelength (λ). The contrast of the Gabors was 0.90. Viewing was monocular, and a chin-and-head rest stabilized the heads of the observers.

Contour integration performance was measured with a temporal 2AFC staircase procedure. The target and nontarget stimuli (a circular contour within the random Gabor field vs. the random field only in detection tasks or circular vs. elliptical contours in discrimination tasks) were separately presented in two stimulus intervals (200 ms each) in a random order separated by a 500-ms interstimulus interval. The observers' task was to judge which stimulus interval contained a contour in detection tasks or the elliptical contour in discrimination tasks. A central fixation cross preceded (350 ms) and stayed through each trial. Auditory feedback was given on incorrect responses. The staircase varied the number of the contour elements in a step size of one contour element. Whenever a contour element was deleted or added, the contour elements were respaced to retain equal spacing. A staircase run consisted of four preliminary reversals and six experimental reversals. A classical 3-down–1-up staircase rule was used, which resulted in a 79.4% convergence level (Levitt, 1971). The mean number of contour elements at six experimental reversals was taken as the threshold element number (N) for each staircase run, based on which a maximal spacing of neighboring contour elements ΔD could be calculated ($\Delta D = 2 \times \pi \times$ eccentricity/N). To allow a comparison between peripheral contour integration measured with stimuli at different spatial scales and retinal eccentricities, we used a contour integration index (CI index), which was maximal spacing in Gabor wavelength (λ) units (CI index = $\Delta D/\lambda$). The same index was once used by Kovacs and Julesz (1993). Indeed, the CI indices measured with stimuli in two different spatial scales at one retinal eccentricity (4°) were similar (Figures 1c and 2c), suggesting that the CI index was an appropriate measure for contour integration performance.

Results

Contour integration in peripheral vision

We initially measured contour integration for detecting a circular contour (Figure 1b) from 1° (fovea) to 35° retinal eccentricity. The spatial frequencies of the contour elements were set at 10.24, 5.12, and 2.56 cpd (using one physically identical set of stimuli at three viewing distances from 6.4 to 1.6 m) for 1°, 2°, and 4° retinal eccentricities, respectively, and at 6.4, 1.3, and 0.94 cpd (using another physically identical set of stimuli at three viewing distances from 1.64 to 0.164 m) for 4°, 20°, and 35° retinal eccentricities, respectively. This spatial frequency arrangement ensured individual contour elements that were highly visible at the stimulus contrast (0.90) used in our experiments (but we later realized that a 10.24 cpd spatial frequency for the foveal stimuli was still too high and caused an unexpected adaptation problem, see below) and, in the meantime, allowed sufficient numbers of contour elements at each retinal eccentricity for accurate measurement of contour integration performance. At 4° retinal eccentricity contour integration was measured with both sets of stimuli at 2.56 and 6.4 cpd, respectively, which made contour integration measured with stimuli at different spatial scales directly comparable.

The results (Figure 1c) showed nearly constant CI indices from 2° to 35° retinal eccentricity, $F(3,9) = 0.568$, $p = .650$. This finding confirmed our initial suspicion that previously reported poor peripheral performance might be limited to the snake contour stimuli rather than to a general absence or decline of contour integration in peripheral vision. Even so, such uncompromised contour integration in the visual periphery up to 35° retinal eccentricity was still very impressive! The same results also showed poorer contour integration in the fovea (1° retinal eccentricity), $F(1,3) = 31.0$, $p = .011$, which might be related to strong adaptation reported by the observers, which, in turn, was likely caused by the high spatial frequency (10.24 cpd) used in this location. A control experiment using lower spatial frequencies (8, 4, and 2 cpd for 1°, 2°, and 4° retinal eccentricities, respectively) revealed similar CI indices from foveal (1°) to 35° retinal eccentricity, $F(4,8) = 0.735$, $p = .593$ (Figure 1d).

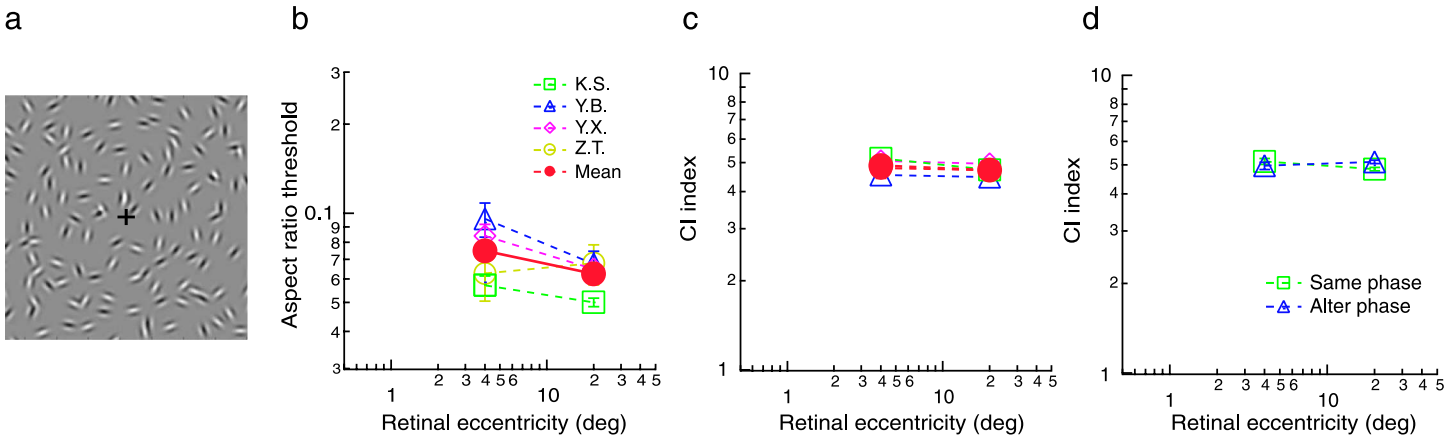

Figure 2. Contour integration for discrimination in peripheral vision. (a) Stimuli used in contour discrimination experiment: an elliptical contour imbedded in a random Gabor noise field. The ellipse rotated from trial to trial through axis orientation jitter. (b) ARTs for elliptical contours at 4° and 20° retinal eccentricities. (c) Contour integration for circular and elliptical discrimination at 4° and 20° retinal eccentricities. The aspect ratios of elliptical contours were set at 1 + 1.5 × ARTs. (d) The effect of relative phase between neighboring contour elements on contour discrimination at 4° and 20° retinal eccentricities averaged from three additional observers (same as in Figure 1e).

We also ran an additional control, comparing the detection of contour stimuli that consist of alternating-phase elements, which were used throughout our study, and those consisting of same-phase elements (all contour and background Gabor elements having identical bright centers and dark sides) in three additional observers at 4°, 20°, and 35° retinal eccentricities. This control experiment revealed no evidence for significant phase effects on contour integration, $F(1,3) = 3.552$, $p = .156$ (Figure 1e), confirming the report of Nugent et al. (2003).

Besides contour detection, we also ran a contour discrimination task in which CI indices were measured when the observers were discriminating the above circular contour (Figure 1b) from an elliptical contour (Figure 2a). The elliptical contour had a slightly suprathreshold aspect ratio and rotated from trial to trial through axis orientation jitter. This task avoided a potential local orientation cue problem in a circular contour detection task, in that contour elements in a specific segment of a circular contour had fairly constant orientations, and the observers might learn to detect these local orientation cues to perform the task even after a contour percept had vanished. However, such local orientation cues barely existed in the circular and elliptical contour discrimination task because the orientations of local contour elements in the same stimulus area were similar. Specifically, we first measured the observers' aspect ratio thresholds (ARTs) for circular and elliptical contour discrimination at 4° and 20° retinal eccentricities using a 2AFC 3-down–1-up staircase method. The spatial frequencies of the contour elements were set at 6.4 and 1.3 cpd for 4° and 20° retinal eccentricities, respectively (same as in Figure 1 for corresponding retinal locations). Each elliptical or circular contour stimulus contained 1.7 times the number of elements at the contour detection threshold obtained from the earlier experiment (Figure 1). Regardless of the aspect ratio, the elliptical contour stimuli in this experiment as well as in subsequent ones had a constant geometric area that was the same as that of the circular contour. The estimated ARTs were 0.075 ± 0.005 and 0.0625 ± 0.003 at 4° and 20° retinal eccentricities, respectively (Figure 2b). We then measured CI indices for circle and ellipse discrimination with the aspect ratios of elliptical contours set at 1 + 1.5 × ARTs. Such a slightly suprathreshold aspect ratio would be sufficient to make the elliptical contours distinct from the circular ones and, in the meantime, would minimize local orientation differences between elliptical and circular contours. The results (Figure 2c) showed similar CI indices (4.89 ± 0.10 vs. 4.72 ± 0.04), $F(1,3) = 4.081$, $p = .137$, at 4° and 20° retinal eccentricities, consistent with data in Figure 1 that peripheral contour integration for our good-Gestalt stimuli was constant across a large area of the visual periphery. The mean CI index for the discrimination task was 4.80, which is poorer than that for the detection task (6.91; Figure 1d), indicating that observers were not based on the sole detection of the circular contour to make circle versus ellipse discrimination when the contour stimuli were near maximal spacing. A control experiment that measured contour discrimination also confirmed that there was no phase effect on contour integration in the discrimination task, $F(1,3) = 1.148$, $p = .363$ (Figure 2d).

The effects of local orientation and position jitter

As contour integration in the fovea (Field et al., 1993), peripheral contour integration was greatly degraded by orientation and position jitters of local contour elements. We measured the effects of orientation and position jitters on contour integration for discrimination at 4° and 20°

retinal eccentricities in three observers. The aspect ratios of the elliptical contours were again set at 1 + 1.5 × ART, and the number of contour elements was 1.3 times the number at maximal spacing for both contours. In the orientation jitter condition, the orientation of each contour element randomly deviated from the contour path from 0° to twice the positive or negative orientation jitter level. In the position jitter condition, each contour element had a random position offset perpendicular to the contour path from 0 to twice the positive or negative position jitter level in λ unit. A 3-up–1-down staircase, which varied the orientation or position jitter level, was used to measure the orientation and position jitter tolerance (threshold). We found that the average orientation jitter tolerance was similar at 4° and 20° retinal eccentricities (12.1 ± 0.54° and 11.6 ± 0.42°, respectively; Figure 3a), $F(1,2) = 0.194$, $p = .70$. The average position jitter tolerance was slightly higher at 20° than at 4° retinal eccentricity (0.74 ± 0.04 vs. 0.67 ± 0.03 in λ units; Figure 3b), $F(1,2) = 34.65$, $p = .028$, which was consistent with the finding of Hess and Dakin (1999) that peripheral contour integration was less affected by local position uncertainty. The position jitter tolerance averaged over two retinal eccentricities converted to an average center-to-center angular deviation of neighboring contour elements from the contour path at 11.0 ± 0.8°, comparable to the average orientation jitter tolerance (11.8 ± 0.8°). These data suggested that the collaboration of neighboring spatial filters with similar (collinear or cocircular) orientation tuning was also critical for contour integration of our good-Gestalt stimuli.

The effects of global position jittering and shape jittering

Uncompromised peripheral contour integration in Figures 1 and 2 was obtained when both the global positions and shapes of our contour stimuli were fixed and known. Besides the good Gestalt nature of our stimuli, how much had the knowledge of contour position and shape contributed to our peripheral contour integration results? The next two experiments would demonstrate that for our contour stimuli, peripheral contour integration was actually unaffected by global position jittering up to 20% of the contour size and by significant shape jittering.

In the global position jitter experiment, we had the same observers perform contour discrimination tasks at 20° retinal eccentricity. The stimuli (circle in one interval and ellipse in the other interval) and procedures were identical to those in the earlier contour discrimination experiment (Figure 1), except that the global positions of two contour stimuli were independently jittered within ±10% and ±20% of the contour radius (±2° and ±4°), respectively, in both horizontal and vertical directions. Our results showed that the ARTs were unaffected by ±10% position jittering but were increased by ±20% position jittering (Figure 4a, left panel). However, after the aspect ratios of elliptical contours under various jittering conditions were normalized by 1 + 1.5 × ART, contour integration (CI index) was practically unchanged by up to ±20% position jittering (Figure 4a, right panel). Position jittering appeared to have more of an effect on shape perception (ARTs) than on contour integration (CI indices).

In the shape jitter experiment, the same observers detected an elliptical contour in a random Gabor field at 20° retinal eccentricity, which appeared in one of two stimulus intervals in a 2AFC trial. The other stimulus interval contains only the random Gabor field. The elliptical contour shape was either fixed or jittered from trial to trial. In the fixed shape condition, the aspect ratio of the elliptical contour was fixed at 1.2 (about 2.9 times mean ART, Figure 2b). In the jittered shape condition, the aspect ratio varied in a wide range from 1.2 to 1.6 (2.9–8.6 times mean ART that was approximately 0.07, Figure 2b) while keeping the geometric

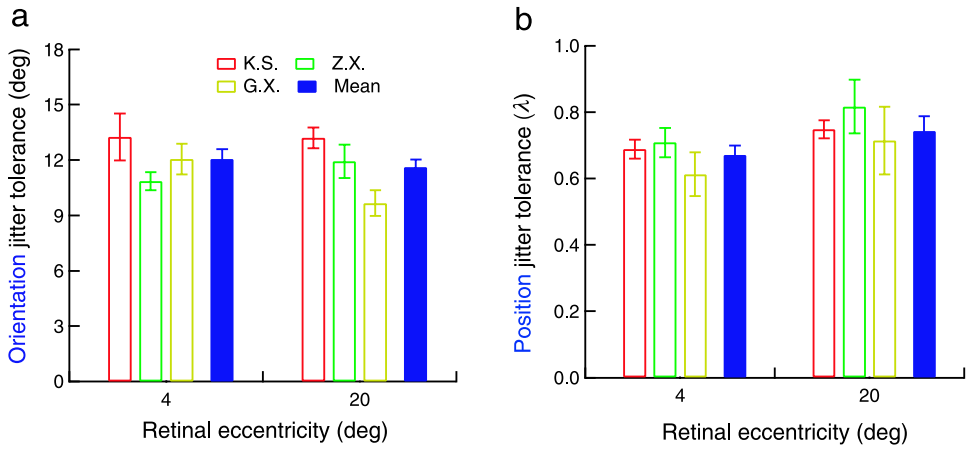

Figure 3. The effects of local orientation and position jitter on peripheral contour integration. (a) Individual and mean tolerance of contour integration to orientation jitter at 4° and 20° retinal eccentricities. (b) Individual and mean tolerance to position jitter at 4° and 20° retinal eccentricities.

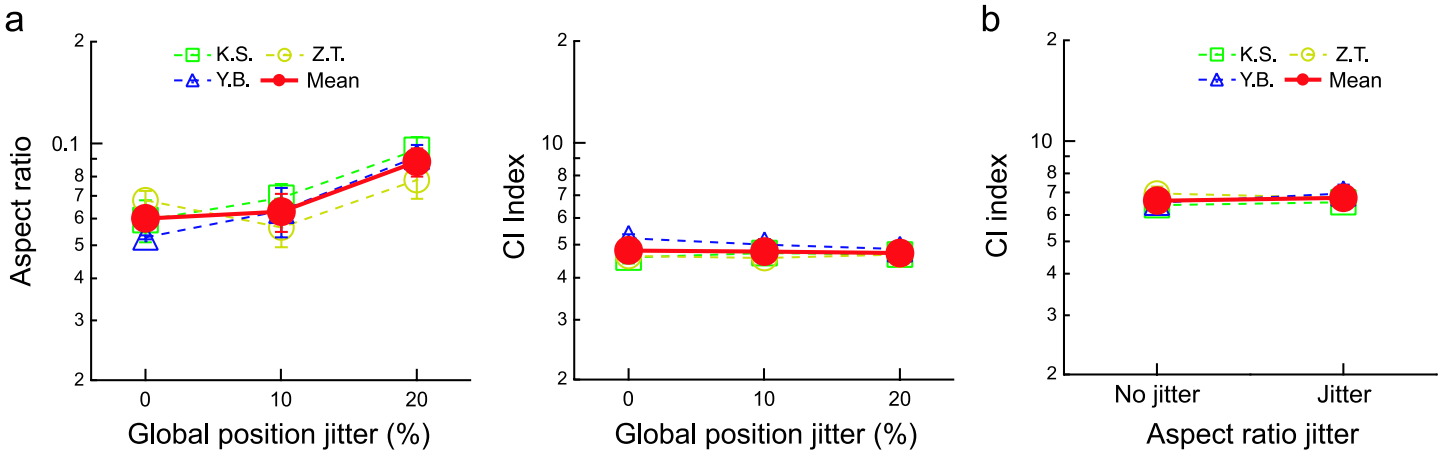

Figure 4. The effects of global position jitter and shape jitter on peripheral contour integration. (a) Left panel: Individual and mean ARTs for ellipse perception with and without global position jitter. Right panel: CI indices for circular and elliptical contour discrimination with and without independent global position jitters of both contours. (b) CI indices for elliptical contour detection with and without aspect ratio jitter.

area constant. The elliptical contour kept rotating from trial to trial as in the earlier experiments. However, the random shape changes due to aspect ratio jitter had no effect on contour integration performance either, $F(1,2) = 0.405$, $p = .590$ (Figure 4b). The mean CI indices were 6.63 ± 0.17 and 6.74 ± 0.18 for fixed and jittered aspect ratio conditions, respectively, discounting the role of shape uncertainty reduction in peripheral contour integration for good-Gestalt stimuli. The CI indices for ellipse detection with or without aspect ratio jitter were actually not different from those for circle detection (6.94 ± 0.20, Figure 1c). These data together indicated that it was the good Gestalt nature of our stimuli, and not stimulus position and shape uncertainty reduction, that was responsible for constant peripheral contour integration.

Contour integration in the lower and upper visual fields

In peripheral vision, many tasks are performed better when the same stimulus pattern is presented in the lower visual field (LVF) than in the upper visual field (UVF; He, Cavanagh, & Intriligator, 1996; Rubin, Nakayama, & Shapley, 1996). Consistent with this asymmetry, the retinotopic presentation of the LVF in V1 is larger (Van Essen, Newsome, & Maunsell, 1984). Would this asymmetry also apply to contour integration? We first measured and discounted asymmetries for contrast thresholds and ARTs in the LVF and UVF so that clean LVF versus UVF contour integration could be compared. Contrast thresholds for a circle (20 elements, mean SF = 1.7 cpd, radius = 7.5°, Figure 5a) centered 15° above or below the fixation cross in a blank field showed larger threshold asymmetry in one observer and less significant asymmetry in the other two, $F(1,2) = 1.074$, $p = .409$ (Figure 5b). In addition, ARTs for discriminating circular and elliptical contours (20 elements, contrasts matched at four times contrast threshold) imbedded in the random Gabor field showed a consistent and significant LVF advantage in all three observers, with the ARTs consistently smaller for the LVF stimuli, $F(1,2) = 45.356$, $p = .021$ (Figure 5c). However, after stimulus contrasts (four times contrast threshold) and aspect ratios ($1 + 1.5 \times$ ART) were matched, contour integration was surprisingly symmetric in the LVF and UVF, $F(1,2) = 0.152$, $p = .734$ (Figure 5d)!

It was unclear what mechanisms could be responsible for this UVF–LVF symmetry. If contour integration occurred in early visual cortex like V1, the equal maximal spacing of contour elements in the UVF and LVF was actually not necessarily inconsistent with a "bigger" V1 representation of the LVF (Van Essen et al., 1984). This could simply be due to the distance in the visual field being scaled with V1 representation so that the equal space between neighboring contour elements could correspond to longer V1 distance for the LVF and shorter V1 distance for the UVF. On the other hand, if contour integration mainly occurred in higher visual areas, neurons with large receptive fields received inputs from multiple V1 neurons and integrated inputs that obey the rules of collinearity and cocircularity to form the percept of continuous contours. Because the input strength from the early visual cortex representing the UVF and LVF had been matched and if these higher visual area neurons had no response bias toward the UVF or UVF inputs, then a UVF–LVF symmetry of contour integration was likely to occur.

Discussion

Our study revealed nearly constant contour integration for shape detection and discrimination from the fovea to up to 35° retinal eccentricity for circular and elliptical

positions of both the circular and elliptical contours were independently jittered up to ±20% of the contour size, which was equivalent to 8° or more than 3 grids (2.4°/grid) in both horizontal and vertical dimensions. This strong trial-by-trial position uncertainty of contour elements would have completely wiped out both local orientation cues and local texture-orientation cues, but we showed that these global position jitters had no significant influence on contour integration (Figure 4a). It was clear that our observers did not use any local cues mentioned above to perform their tasks. They probably had to attend to the entire contours to make decisions.

Besides local cues, the observers might use template matching rather than contour integration to detect well-defined stimuli. During template matching, the brain recognizes an object by comparing it to images of objects already stored in memory. Consistent with many of our findings, a template-matching model would suffer from local orientation and position jitters (Figure 3), and it would be immune to global position jitters (Figure 4a) because the model could easily match the displaced stimuli through image translation. However, template matching was expected to be impaired by contour shape jitters, which contradicted with our aspect ratio jitter data that showed unaffected CI indices (Figure 4b). This inconsistency effectively excluded simple template matching as an alternative mechanism underlying perception of our good-Gestalt contour stimuli.

Acknowledgments

This research was supported by funds from Beijing Normal University and the Chinese Academy of Sciences. We thank Drs. Dennis Levi, Wu Li, and Li Zhaoping for their helpful comments during the preparation of the manuscript.

Commercial relationships: none.
Corresponding author: Cong Yu.
Email: yucong@bnu.edu.cn.
Address: Institute of Cognitive Neuroscience and Learning, Beijing Normal University, Beijing 100875, China.

References

Braun, J. (1999). On the detection of salient contours. *Spatial Vision, 12,* 211–225. [PubMed]

Field, D. J., Hayes, A., & Hess, R. F. (1993). Contour integration by the human visual system: Evidence for a local "association field." *Vision Research, 33,* 173–193. [PubMed]

Geisler, W. S., Perry, J. S., Super, B. J., & Gallogly, D. P. (2001). Edge co-occurrence in natural images predicts contour grouping performance. *Vision Research, 41,* 711–724. [PubMed]

Gilbert, C., Ito, M., Kapadia, M., & Westheimer, G. (2000). Interactions between attention, context and learning in primary visual cortex. *Vision Research, 40,* 1217–1226. [PubMed]

He, S., Cavanagh, P., & Intriligator, J. (1996). Attentional resolution and the locus of visual awareness. *Nature, 383,* 334–337. [PubMed]

Hess, R. F., & Dakin, S. C. (1997). Absence of contour linking in peripheral vision. *Nature, 390,* 602–604. [PubMed]

Hess, R. F., & Dakin, S. C. (1999). Contour integration in the peripheral field. *Vision Research, 39,* 947–959. [PubMed]

Hess, R., & Field, D. (1999). Integration of contours: New insights. *Trends in Cognitive Sciences, 3,* 480–486. [PubMed]

Hess, R. F., Hayes, A., & Field, D. J. (2003). Contour integration and cortical processing. *Journal of Physiology, 97,* 105–119. [PubMed]

Ito, M., & Gilbert, C. D. (1999). Attention modulates contextual influences in the primary visual cortex of alert monkeys. *Neuron, 22,* 593–604. [PubMed] [Article]

Kapadia, M. K., Westheimer, G., & Gilbert, C. D. (2000). Spatial distribution of contextual interactions in primary visual cortex and in visual perception. *Journal of Neurophysiology, 84,* 2048–2062. [PubMed] [Article]

Kovacs, I., & Julesz, B. (1993). A closed curve is much more than an incomplete one: Effect of closure in figure-ground segmentation. *Proceedings of the National Academy of Sciences of the United States of America, 90,* 7495–7497. [PubMed] [Article]

Levitt, H. (1971). Transformed up–down methods in psychoacoustics. *Journal of the Acoustical Society of America, 49*, 467–477. [PubMed]

Li, Z. (1998). A neural model of contour integration in the primary visual cortex. *Neural Computation, 13,* 903–940. [PubMed]

Nugent, A. K., Keswani, R. N., Woods, R. L., & Peli, E. (2003). Contour integration in peripheral vision reduces gradually with eccentricity. *Vision Research, 43,* 2427–2437. [PubMed]

Orbach, H. S., & Wilson, H. R. (1999). Factors limiting peripheral pattern discrimination. *Spatial Vision, 12,* 83–106. [PubMed]

Pettet, M. W. (1999). Shape and contour detection. *Vision Research, 39,* 551–557. [PubMed]

Pettet, M. W., McKee, S. P., & Grzywacz, N. M. (1998). Constraints on long range interactions mediating contour detection. *Vision Research, 38,* 865–879. [PubMed]

Rubin, N., Nakayama, K., & Shapley, R. (1996). Enhanced perception of illusory contours in the lower versus upper visual hemifields. *Science, 271,* 651–653. [PubMed]

Sigman, M., Cecchi, G. A., Gilbert, C. D., & Magnasco, M. O. (2001). On a common circle: Natural scenes and Gestalt rules. *Proceedings of the National Academy of Sciences of the United States of America, 98,* 1935–1940. [PubMed] [Article]

Tversky, T., Geisler, W. S., & Perry, J. S. (2004). Contour grouping: Closure effects are explained by good continuation and proximity. *Vision Research, 44,* 2769–2777. [PubMed]

Van Essen, D. C., Newsome, W. T., & Maunsell, J. H. (1984). The visual field representation in striate cortex of the macaque monkey: Asymmetries, anisotropies, and individual variability. *Vision Research, 24,* 429–448. [PubMed]